MATHEMATICAL BIOSCIENCES
AND ENGINEERING
Volume **10**, Number **2**, April **2013**

doi:10.3934/mbe.2013.10.319

pp. **319–344**

MODELING OF THE KINETICS OF VITAMIN D_3 IN OSTEOBLASTIC CELLS

Robert P. Gilbert, Philippe Guyenne and Ying Liu

Department of Mathematical Sciences
University of Delaware
Newark, DE 19716, USA

(Communicated by Stephen Cantrell)

Abstract. A one-dimensional model for the transport of vitamin D_3 in an osteoblast cell is proposed, from its entry through the membrane to its activation of RANKL synthesis in the nucleus. In the membrane and cytoplasm, the transport of D_3 and RANKL is described by a diffusion process, while their interaction in the nucleus is modeled by a reaction-diffusion process. For the latter, an integral equation involving the boundary conditions, as well as an asymptotic solution in the regime of small concentrations, are derived. Numerical simulations are also performed to investigate the kinetics of D_3 and RANKL through the entire cell. Comparison between the asymptotics and numerics in the nucleus shows an excellent agreement. To our knowledge, this is the first time, albeit using a simple model, a description of the complete passage of D_3 through the cell membrane, the cytoplasm, into the cell nucleus, and finally the production of RANKL with its passage to the exterior of the cell, has been modeled.

1. **Introduction.** Bone is a composite structure of living cells embodied in an organic, highly mineralized matrix. Bone is built during body growth by bone-building cells, called osteoblasts, that synthesize and release organic molecules, largely collagen. This constitutes the matrix onto which a variety of calcium salts are deposited. The mature calcium salt is carbanato-hydroxyapatite. Bone is resorbed by osteoclasts, cells that form a podosome, a tent-like membrane cover over the bone surface into the space of which they secrete enzymes and hydrogen ions, the combined action of which leads to mineral dissolution and matrix destruction. Adult bone undergoes remodeling, i.e. resorption by osteoclasts, followed by renewed matrix synthesis and mineral deposition initiated by osteoblasts. Two types of bone mineral structure are known: trabecular and compact. Trabecular bone, approximately 20% of total adult bone, has struts and undergoes renewal at about twice the rate of compact bone. It is trabecular bone that is primarily destroyed in postmenopausal osteoporosis. Total bone renewal, i.e. trabecular and compact averaged out, approximates 3.6% per year.

Bone formation is tightly regulated by the cells present inside the bone. Especially two key players, osteoclasts (bone resorbing cells) and osteoblasts (bone forming cells), tightly regulate the amount of bone matrix. The balance between

2010 *Mathematics Subject Classification.* Primary: 58F15, 58F17; Secondary: 53C35.

Key words and phrases. RANKL, receptors, osteoblasts, reaction-diffusion, numerical simulations.

active osteoblasts and osteoclasts is crucial for proper bone formation and maintenance. 1,25-Dihydroxyvitamin D_3, the active form of vitamin D_3, plays a critical role during bone formation. As illustrated in Figure 1, it regulates the differentiation of hematopoietic stem cells and preosteoblasts into osteoclast progenitor cells and mature osteoblasts (see [3] for further details). It also induces osteoclast differentiation from the osteoclast progenitor cell to the prosteoclast by affecting the RANKL/RANK/OPG axis, by upregulation of RANKL. This enables the binding of RANKL to RANK leading to the differentiation of the osteoclast progenitor. 1,25-Dihydroxyvitamin D_3 also stimulates the secretion of collagenase, osteopontin, C3, MGP and plasminogen, which in turn affect osteoclast differentiation.

In this paper, we propose a reasonably complete biological model of the preosteoblastic cell and a simplified mathematical version for the transport of vitamin D_3 from its entry through the membrane surface to its activation of RANKL synthesis in the nucleus. We indicate where we deviate from the biological system in this initial attempt and where we might provide a more complete mathematical version. The outgoing transport of RANKL from the nucleus to the membrane is also described. Assuming spherical symmetry, the cell is defined by a one-dimensional domain divided into three regions: the nucleus, the cytoplasm and the membrane. In each region, the transport of D_3 and RANKL is modeled by a diffusion process with distinct properties. For the interaction problem in the nucleus, we derive a simple integral equation involving the boundary conditions. We also identify an asymptotic regime of parameters that allows us to linearize the nonlinear partial differential equations of the nuclear model and derive an approximate analytical solution. For the kinetics through the entire cell, we perform numerical simulations based on a finite-difference scheme, which show that the various transport and synthesis processes are well reproduced in the context of our model. The asymptotic solution for the nucleus is also compared with the numerical solution, and a very good agreement is found.

The remainder of the paper is organized as follows. In Section 2, we describe the mathematical model for the kinetics of D_3 and RANKL in an osteoblast cell, including the diffusion equations in the membrane and cytoplasm, and the reaction-diffusion equations in the nucleus. The integral equation together with the asymptotic solution of the nuclear model are derived in Section 3, and details are given in the Appendix. Numerical simulations of the full cellular model are presented in Section 4, including a description of the numerical methods and a discussion of the numerical results. Finally, concluding remarks are given in Section 5.

2. **Mathematical model.**

Typically, the vitamin D serum binding proteins, exterior to the cell, are present at high concentrations and have high off rates relative to the membrane receptors, VDR_m, [1] that are present at much lower concentrations but have higher binding affinities. These receptors are fast (seconds-minutes) and mediate catabolic effects. There is also a nuclear receptor, VDR_n, in osteoblast cells that responds to D_3, which is a slow (hours), non-calcemic receptor mediating anabolic effects.

Vitamin D_3 dissociates from the serum binding vitamin D_3 protein (DBP) to the membrane receptor, acting as a molecular switch for the activation of VDR_n. This

[1]The membrane associated rapid response to steroids specific for vitamin D is also known as MARRS [14].

then activates responsive genes. In the model, for simplicity, we choose VDR_n to be located in the nucleus rather than in the cytoplasm.

VDR_m then signals VDR_n to shut down the production of OPG and promotes transcription of the gene encoding receptor activator of RANKL [23]. Osteoclastogenesis can be inhibited by osteoprotegerin, OPG or RANKL, in their capacity acting as a decoy receptor for RANKL [23]. Shutting down OPG is essential to decreasing the maturation and metabolic effects of osteoclasts, resulting in a decrease of bone resorption. The RNA encoding RANKL or OPG is exported to the cytoplasm where it is translated into protein on the ribosome. The new protein is then inserted into the secretory pathway for export. The mechanism by which RANKL is converted from a membrane to a soluble structure is unclear.

2.1. **Assumptions concerning the model.**

- The process of serum binding proteins passing along the hormone from one to the next through a sequence of low affinity binding and release events [2] (the buckets) until reaching the target (the receptor) is modelled by a sequence of short distance diffusional events with a pause in between each. The length of the pause (binding event) determines the rate of the movement of the diffusing molecule. When the molecule binds to the receptor, the number of molecules that enters is determined by the number of liganded receptors. In this paper we eliminated this step as the mathematical model was sufficiently complicated for an initial attempt. It will be included, however in subsequent models.
- When D_3 interacts with MARRS, the membrane diffusion coefficient changes from a high off-rate to a lower value that allows a specific amount of D_3 to cross the membrane. Once transfer is completed, the diffusion coefficient reverts to the high off-value and transmembrane transfer is turned off.
- The saturation curve for the membrane receptor is biphasic.This means two separate events may be initiated, such as opening a calcium channel and permitting D_3 to pass through the membrane. Calcium activates and, at greater concentration, deactivates transcription. These events are symbolized by changes in the kinetic coefficients.
- Calcium entering the cells initiates cross talk between the vesicles and the nuclear receptor via signal transduction pathways. We assume that this switching mechanism is located in the nuclear receptor, as nuclear receptor regulated genes still turn on in 24 hrs when the membrane system is blocked. This is modeled using a threshold concerning the number of occupied nuclear receptors.
- The translocation of vitamin D_3 to the nucleus occurs using a chaperon, DBP, that moves along cytoskeletal tracks through the cytoplasm [17] and then diffuses into the nucleus to reach the VDR_n. However, in the present model this is described by a diffusion process.
- The binding with VDR_n is described by a reaction-diffusion equation that is initiated by the signal cross-talk with MARRS. Signaling from the membrane receptor to the nuclear receptor depends on a threshold effect that induces a change in the kinetics of the nuclear response, with a time lag before the signal is received. In the present mathematical model the reaction-diffusion

[2]This has been spoken of as an intracellular bucket brigade where the hormone moves from one binding protein to the next [2].

equation becomes valid upon the arrival of the D_3. This is appropriate as we use a diffusion model in the cytoplasm rather than transportation along microtubules.

- D_3 combines with the nuclear receptor and diffuses to the nucleus where it initiates, by a hormone-like action, the target gene response. The effect of this response may be slow, requiring hours.
- Biosynthesis of soluble RANKL is a multistep process, but will be modeled as a single step. RANKL is a soluble decoy that is assumed to diffuse through the nuclear space into the cytoplasm from which it exits through the membrane into the body fluids.

2.2. **Membrane-cytoplasm model.** Assume that the cell is a small ball with radius $r_m^e > 0$ (Figure 2), the cell membrane is a spherical shell, and also assume that the diffusion of vitamin D_3 ($1{,}25(OH)_2D_3$) from the membrane to the nucleus is independent of the spherical angles (θ, ϕ). Then we can model the interaction of the $1{,}25(OH)_2D_3$ and the receptors by a system of partial differential equations in one space dimension.

In the following, we represent the membrane receptor, VDR_m, by M and the compound formed from D_3 and VDR_m by $D * M$. The genes for both OPG and RANKL are regulated by the nuclear receptor for D_3 and this is described in a subsequent section. It is proposed that the VDR_m complex that regulates calcium signaling also regulates the intake of D_3 into the cell.

One possibility is to model the entry of D_3 into the cell by having the diffusion coefficient for the membrane dependent on the concentration of $D * M$. This is a transient phenomenon, namely increasing D_3 in the serum suddenly above its basal concentration leads MARRS to signal ER, allowing an increased flow of Ca^{2+} into the cell. This in turn signals a temporary change in the membrane diffusion coefficient

$$\kappa_m(D * M) = \begin{cases} \kappa_m^H & \text{for high intake} \\ \kappa_m^L & \text{for low intake} \end{cases},$$

which then after a fixed time reverts to its non-entry state. Another possibility is to have D_3 collect in caveolae and have MARRS using Ca^{2+} to signal dynamin to snip the vesicle containing D_3. At this point, it is unknown exactly how D_3 enters the cell. We assume that MARRS signals the nuclear receptor using Ca^{2+}, which also signals the entry of D_3. Hence, in some way, the concentration of Ca^{2+} is tied to the entry of D_3 into the cell. We make the simplifying assumption that the boundary condition for D_3 is proportional to Ca^{2+}. We use the single-pool model for intracellular Ca^{2+} from [1] to describe the calcium spiking. These spikes, when they become large enough, switch the membrane diffusion coefficient from *off* to *on*, etc. In this paper, we simplify the mechanism by assuming the flow of D_3 into the membrane is proportional to that of Ca^{2+}.

In the membrane, we represent the concentration of D_3 by the function $D_m(r, t)$. We model the transport of D_3 through the membrane of the cell by a diffusion process where the diffusion coefficient is chosen to match the time scale necessary to pass the correct amount through the membrane during the time it is open. After this time, the diffusion coefficient changes to permit essentially no D_3 to pass through the membrane. As mentioned in the previous section, this is controlled by MARRS. In this section, we provide the analysis for the case where we either increase or decrease the concentration of D_3 in the serum. When the membrane diffusion

coefficient has switched to its higher value κ_m^H, $D_m(r,t)$ satisfies the equation

$$\kappa_m \frac{\partial^2 D_m}{\partial r^2} = \frac{\partial D_m}{\partial t}, \quad r_m^i < r < r_m^e. \tag{2.1}$$

In this paper, we assume that D_3 obeys a diffusion law in the cytoplasm rather than being transported along microtubules in the cytoplasm, namely

$$\kappa_c \frac{\partial^2 D_c}{\partial r^2} = \frac{\partial D_c}{\partial t}, \quad r_n < r < r_m^i.$$

Accurate measurements of D_3 transport in osteoblast cells are usually difficult to obtain. According to [18], the effective diffusion constant might be described by a two-parameter power law. In [22], transport along microtubules or actin filaments is compared. The microtubules are for long-range transport whereas the actin filaments are for local movement of organelles. This is a possibility we might try in the future; however for the present, we use diffusion transport, estimating κ_c by Einstein's formula

$$\kappa_c = \frac{k_B T}{6\pi\eta r_D}, \tag{2.2}$$

where k_B is Boltzmann's constant, η the dynamic viscosity of water and $T = 309$ K (internal body temperature). Assuming spherical symmetry for the D molecule, its radius is given by

$$\begin{aligned} r_D &= 0.066\, m_D^{1/3}, \\ &= 4.9294 \times 10^{-10}\,\mathrm{m} = 0.4929\,\mathrm{nm}, \end{aligned} \tag{2.3}$$

where $m_D = 416.64$ g mol^{-1} is the molecular mass of $1{,}25(OH)_2D_3$. As discussed above, because diffusion is strong in the membrane during the Ca^{2+} influx, we choose $\kappa_m = 10\kappa_c$.

We match the membrane and cytoplasm solutions at the inner membrane surface $r = r_m^i$, using the transmission conditions:

$$D_c(r_m^{i,-},t) = D_m(r_m^{i,+},t), \quad \kappa_c \frac{\partial D_c}{\partial r}(r_m^{i,-},t) = \kappa_m \frac{\partial D_m}{\partial r}(r_m^{i,+},t). \tag{2.4}$$

At the external membrane surface $r = r_m^e$, we assume the *effective* concentration is proportional to the Ca^{2+} spikes as described in [1]. These Ca^{2+} spikes obey the system of ordinary differential equations

$$\frac{dD_m}{dt} = J_{channel} - J_{pump} + J_{leak}, \tag{2.5}$$

$$\tau_n \frac{dn}{dt} = n_\infty(D_m) - n, \tag{2.6}$$

where

$$\begin{aligned} J_{channel} &= k_{flux}\,\mu([IP_3])\,n\left(b + \frac{V_1 D_m}{k_1 + D_m}\right), \\ J_{pump} &= \frac{\gamma D_m}{k_\gamma + D_m}, \\ J_{leak} &= \beta, \\ n_\infty(D_m) &= 1 - \frac{D_m^2}{k_2^2 + D_m^2}, \\ \mu([IP_3]) &= \mu_0 + \frac{\mu_1[IP_3]}{k_\mu + [IP_3]}. \end{aligned} \tag{2.7}$$

Parameter	Value
b	0.111
V_1	0.889
β	$0 - 0.02$ μM s^{-1}
γ	2.0 μM s^{-1}
τ_n	2.0 s
k_1	0.7 μM s^{-1}
k_γ	0.1 μM
k_2	0.7 μM
k_{flux}	8.1 μM s^{-1}

TABLE 1. Parameter values in the boundary conditions (2.5)–(2.7) at the external membrane surface. b represents a basal current through the Ca^{2+} channel. V_1 is the proportion of IP_3Rs that are activated by the binding of Ca^{2+}. β is the constant rate of Ca^{2+} influx into the cytosol. γ is the maximum rate of Ca^{2+} pumping from the cytosol. k_γ is the concentration of Ca^{2+} at half-maximum pumping. τ_n is the time constant for the dynamics of n. k_{flux} is the maximum total Ca^{2+} flux through all IP_3Rs. Further details can be found in [1].

Each J term represents a concentration flux, n is the dimensionless variable representing the proportion of receptor IP_3Rs that have been filled by Ca^{2+}, n_∞ denotes the steady state of n as a function of D_m, $\mu([IP_3])$ is the proportion of IP_3Rs that have their IP_3 binding domain activated, and $b + V_1 = 1$. The values of the constants in (2.6)–(2.7) are taken from [1] and listed in Table 1. A numerical simulation of (2.5)–(2.7), starting from zero initial conditions and using the 4th-order Runge–Kutta method, is depicted in Figure 3.

2.3. **Nuclear model.** It is assumed that the nucleus is a smaller concentric ball of radius r_n. Let D_n denote the concentration of D_3 in the nucleus, N the concentration of VDR_n and $V_n = D_n * N$ the compound formed with the nuclear receptor. Their kinetics may be described by the reaction diagram

$$\begin{array}{ccccc} \text{influx} & & & & \\ \downarrow & & k_3 & & \\ D_n + & N & \rightleftharpoons & D_n * N & \\ & & k_4 & & \\ \downarrow & & & & \\ \text{diffusion} & & & & \end{array}$$

Considering again isotropy, we model their dynamics as a reaction-diffusion process of the form

$$\frac{\partial D_n}{\partial t} = \kappa_n \frac{\partial^2 D_n}{\partial r^2} + k_4 V_n - k_3 (R_N - V_n) D_n, \tag{2.8}$$

$$\frac{\partial V_n}{\partial t} = \kappa_{vn} \frac{\partial^2 V_n}{\partial r^2} - k_4 V_n + k_3 (R_N - V_n) D_n, \tag{2.9}$$

Parameter	Value
k_3	6.7×10^{-9} pM^{-1} s^{-1}
k_4	1.96×10^{-7} s^{-1}
R_N	10 pM

TABLE 2. Parameter values in the nuclear model (2.8)–(2.9). k_3 is the rate of RANK-RANKL binding. k_4 is the rate of RANK-RANKL unbinding. R_N is a fixed concentration of RANK. Further details can be found in [13].

where k_3, k_4 and R_N are taken from [13]. The values of these parameters, together with their description, are given in Table 2. We choose $\kappa_n = 0.1\kappa_c$ to allow for a sufficient level of D in the nucleus so it can produce enough V to diffuse out, in a reasonable amount of time.

At the surface $r = r_n$ of the nucleus, we have the transmission conditions

$$D_n(r_n^-, t) = D_c(r_n^+, t), \quad \kappa_n \frac{\partial D_n}{\partial r}(r_n^-, t) = \kappa_c \frac{\partial D_c}{\partial r}(r_n^+, t),$$

and, at the center $r = 0$, we impose the reflecting condition

$$\kappa_n \frac{\partial D_n}{\partial r}(0, t) = \kappa_{vn} \frac{\partial V_n}{\partial r}(0, t) = 0,$$

which is a suitable choice of boundary condition at this location given the spherical symmetry adopted in the problem.

The initial conditions are simply

$$D_n(r, 0) = D_c(r, 0) = D_m(r, 0) = 0, \quad 0 < r < r_m^e. \tag{2.10}$$

2.4. **Outgoing compound.** In the previous section, we define the compound RANKL formed with the nuclear receptor by $V_n := D_n * N$. Assume that D_n combines with the nuclear receptor and diffuses to the cytoplasm when it initiates. Let V_c denote the concentration of RANKL in the cytoplasm and V_m the concentration in the membrane. This step is modelled as a diffusion process by the following equations:

$$\kappa_{vc} \frac{\partial^2 V_c}{\partial r^2} = \frac{\partial V_c}{\partial t}, \quad r_n < r < r_m^i,$$

and

$$\kappa_{vm} \frac{\partial^2 V_m}{\partial r^2} = \frac{\partial V_m}{\partial t}, \quad r_m^i < r < r_m^e,$$

where κ_{vc} and κ_{vm} are the diffusion coefficients in the cytoplasm and membrane, respectively. Applying again formula (2.3) to the V molecule, we estimate its radius to be

$$r_V = 1.8465 \times 10^{-9}\,\text{m} = 1.8465\,\text{nm},$$

which is about four times larger than r_D, using the molecular mass $m_V = 21900$ g mol^{-1} of RANKL. Since the V molecule is bigger than the D molecule, we expect its dispersion to be slower. We thus choose

$$\kappa_{vn} = \frac{1}{4}\kappa_n, \quad \kappa_{vc} = \frac{1}{4}\kappa_c, \quad \kappa_{vm} = \frac{1}{4}\kappa_m,$$

Parameter	Value
κ_n	6.559×10^{-11} m^2 s^{-1}
κ_c	6.559×10^{-10} m^2 s^{-1}
κ_m	6.559×10^{-9} m^2 s^{-1}
κ_{vn}	1.639×10^{-11} m^2 s^{-1}
κ_{vc}	1.639×10^{-10} m^2 s^{-1}
κ_{vm}	1.639×10^{-9} m^2 s^{-1}

TABLE 3. Diffusion coefficients for D and V based on Einstein's formula (2.2). We use $k_B = 1.3806488 \times 10^{-23}$ J K^{-1}, $T = 309$ K and $\eta = 0.7 \times 10^{-3}$ N s m^{-2}.

because the diffusion coefficient is inversely proportional to the molecular radius by virtue of (2.2). The values of the various diffusion coefficients for D and V are summarized in Table 3.

At the interfaces between the nucleus and cytoplasm, and between the cytoplasm and membrane, we have the following transmission conditions:

$$V_n(r_n^-, t) = V_c(r_n^+, t), \quad \kappa_{vn}\frac{\partial V_n}{\partial r}(r_n^-, t) = \kappa_{vc}\frac{\partial V_c}{\partial r}(r_n^+, t), \tag{2.11}$$

and

$$V_c(r_m^{i,-}, t) = V_m(r_m^{i,+}, t), \quad \kappa_{vc}\frac{\partial V_c}{\partial r}(r_m^{i,-}, t) = \kappa_{vm}\frac{\partial V_m}{\partial r}(r_m^{i,+}, t).$$

At the external boundary of the membrane, we consider the fast diffusion case assuming that there is no build-up, namely

$$V_m(r_m^e, t) = 0.$$

The initial conditions are given by

$$V_n(r, 0) = V_c(r, 0) = V_m(r, 0) = 0, \quad 0 < r < r_m^e. \tag{2.12}$$

3. **Asymptotic solution of the nuclear model.** The reaction-diffusion model (2.8)–(2.10), (2.11) and (2.12) for D_n and V_n in the nucleus is a nonlinear system of partial differential equations. In this section, we derive a first-order analytical solution in an asymptotic regime with prescribed fluxes through the surface of the nucleus. We first examine the case of constant fluxes and then extend the solution to time-dependent fluxes.

Consider a closed version of this reaction-diffusion model in the form

$$\begin{aligned} \frac{\partial D_n}{\partial t} &= \kappa_n \frac{\partial^2 D_n}{\partial r^2} + k_4 V_n - k_3(R_N - V_n)D_n, \\ \frac{\partial V_n}{\partial t} &= \kappa_{vn}\frac{\partial^2 V_n}{\partial r^2} - k_4 V_n + k_3(R_N - V_n)D_n, \end{aligned}$$

with initial conditions

$$D_n(r, 0) = V_n(r, 0) = 0, \tag{3.1}$$

and boundary conditions

$$\frac{\partial D_n}{\partial r}(0, t) = \frac{\partial V_n}{\partial r}(0, t) = 0, \tag{3.2}$$

$$\frac{\partial D_n}{\partial r}(r_n, t) = g(t), \quad \frac{\partial V_n}{\partial r}(r_n, t) = h(t), \tag{3.3}$$

where $g(t)$ and $h(t)$ are prescribed fluxes at $r = r_n$, which are assumed to be smooth functions.

The first step is to identify a suitable asymptotic regime with a small parameter. For this purpose, we non-dimensionalize the equations by introducing the dimensionless variables

$$D' = \frac{D_n}{\mathcal{D}}, \quad V' = \frac{V_n}{\mathcal{D}}, \quad t' = \frac{t}{\mathcal{T}}, \quad r' = \frac{r}{\mathcal{R}},$$

with the characteristic values

$$\mathcal{D} = \mathcal{D}_0 \frac{k_4}{k_3}, \quad \mathcal{R} = r_n, \quad \mathcal{T} = \frac{\mathcal{R}^2}{\kappa_n}, \tag{3.4}$$

where $\mathcal{D}_0 \ll 1$ is a dimensionless scaling factor. Dropping the primes, the non-dimensionalized version of (2.8)–(2.9) reads

$$\frac{\partial D}{\partial t} = \frac{\partial^2 D}{\partial r^2} - aD + bV + \epsilon DV, \tag{3.5}$$

$$\frac{\partial V}{\partial t} = \alpha \frac{\partial^2 V}{\partial r^2} + aD - bV - \epsilon DV, \tag{3.6}$$

where

$$\alpha = \frac{\kappa_{vn}}{\kappa_n}, \quad a = \frac{R_N k_3 \mathcal{R}^2}{\kappa_n}, \quad b = \frac{k_4 \mathcal{R}^2}{\kappa_n}, \quad \epsilon = \frac{\mathcal{D}_0 k_4 \mathcal{R}^2}{\kappa_n}.$$

The values of these dimensionless constants are listed in Table 4. Clearly, diffusion is the dominant process for both D and V, the other effects being much weaker. We note that a and b are comparable while $\epsilon \ll a, b$ (because $\epsilon = \mathcal{D}_0 b$ and $\mathcal{D}_0 \ll 1$). This suggests that ϵ can be used as a small parameter in perturbation calculations, and thus the nonlinear terms in (3.5)–(3.6) can be neglected as compared to the linear terms. We could in fact only retain the diffusive terms and neglect all other terms in good approximation. It turns out however that the linear terms in factor of a and b can be solved exactly together with the diffusive terms, as shown below. Moreover, these linear terms in factor of a and b represent the leading-order contributions to the reaction process, and thus they should be taken into account. The scaling $\mathcal{D}_0 \ll 1$ may be viewed as a regime of 'small' concentration, which is a reasonable choice given the fact that only a fraction of the vitamin D_3 serum eventually gets into the nucleus to activate the production of RANKL.

In order to solve the pair of nonlinear partial differential equations (3.5)–(3.6), we need to find a scheme by which to do so. As there is not one in the mathematical literature, we list our results here formally as *Theorems* (see in particular Theorem 3.1)These results are formal and may be of slight interest to biologists, in which case we urge the reader to pass over them. They are added to the paper, nevertheless, for completeness.

Theorem 3.1. *Let $g(t)$ and $h(t)$ in (3.3) be two integrable functions of t, and define*

$$E(t) = \int_0^{r_n} (D + V) dr.$$

Then the solution (D, V) of (3.5)–(3.6) with initial conditions (3.1) and boundary conditions (3.2)–(3.3) satisfies the integral equation

$$E(t) = \int_0^t [g(\tau) + \alpha h(\tau)] \, d\tau. \tag{3.7}$$

Proof. The coupling terms can be eliminated by adding (3.5)–(3.6) together, yielding

$$\frac{\partial D}{\partial t} + \frac{\partial V}{\partial t} = \frac{\partial^2 D}{\partial r^2} + \alpha \frac{\partial^2 V}{\partial r^2}.$$

Then integrating in r and using the boundary conditions (3.2)–(3.3), we obtain

$$\begin{aligned} \int_0^{r_n} \frac{\partial}{\partial t}(D+V)dr &= \int_0^{r_n} \left(\frac{\partial^2 D}{\partial r^2} + \alpha \frac{\partial^2 V}{\partial r^2} \right) dr, \\ &= \left[\frac{\partial D}{\partial r} + \alpha \frac{\partial V}{\partial r} \right]_0^{r_n}, \\ &= g(t) + \alpha h(t). \end{aligned}$$

Differentiation in t and integration in r can be interchanged on the left-hand side of the above equation. Finally, integrating in t and using the initial conditions (3.1), we arrive at

$$\int_0^{r_n} (D+V)dr = \int_0^t \left[g(\tau) + \alpha h(\tau) \right] d\tau.$$

In the case where $g(t) = h(t) = 1$, this equation reduces to

$$\int_0^{r_n} (D+V)dr = (1+\alpha)t,$$

which concludes the proof of the theorem. □

An asymptotic solution can be found by regular perturbation in the form of a power series in ϵ,

$$D(r,t) = \sum_{j=0}^{\infty} \epsilon^j D^{(j)}(r,t), \tag{3.8}$$

$$V(r,t) = \sum_{j=0}^{\infty} \epsilon^j V^{(j)}(r,t). \tag{3.9}$$

Plugging (3.8)–(3.9) in (3.5)–(3.6), and in the initial and boundary conditions, the first-order solution $(D^{(0)}, V^{(0)})$ satisfies the linear system

$$\frac{\partial D^{(0)}}{\partial t} = \frac{\partial^2 D^{(0)}}{\partial r^2} - aD^{(0)} + bV^{(0)}, \tag{3.10}$$

$$\frac{\partial V^{(0)}}{\partial t} = \alpha \frac{\partial^2 V^{(0)}}{\partial r^2} + aD^{(0)} - bV^{(0)}, \tag{3.11}$$

with

$$D^{(0)}(r,0) = V^{(0)}(r,0) = 0, \tag{3.12}$$

and

$$\begin{gathered} \frac{\partial D^{(0)}}{\partial r}(0,t) = \frac{\partial V^{(0)}}{\partial r}(0,t) = 0, \\ \frac{\partial D^{(0)}}{\partial r}(r_n,t) = g(t), \quad \frac{\partial V^{(0)}}{\partial r}(r_n,t) = h(t). \end{gathered} \tag{3.13}$$

Note the non-homogeneity in the boundary conditions (3.13). Although the linear system (3.10)–(3.13) is a simplification of the nuclear model, it still exhibits important features of the interaction problem, due to the linear coupling terms. Clearly, the asymptotic solution $(D^{(0)}, V^{(0)})$ also satisfies the integral equation (3.7), as can be shown by following the proof of Theorem 3.1.

In the case of constant fluxes at $r = r_n$, say $g(t) = h(t) = 1$ for simplicity, we have the following result:

Parameter	Value
α	0.25
a	4.08×10^{-7}
b	1.19×10^{-6}
ϵ	1.19×10^{-8}

TABLE 4. Parameter values in the non-dimensionalized nuclear model (3.5)–(3.6). We use $r_n = 2 \times 10^{-5}$ m and $\mathcal{D}_0 = 10^{-2}$.

Theorem 3.2. *Let $g(t) = h(t) = 1$ in (3.13). Assume $(D^{(0)}, V^{(0)})$ is a series solution of the linear problem (3.10)–(3.13). Then this solution can be written as*

$$\begin{pmatrix} D^{(0)}(r,t) \\ V^{(0)}(r,t) \end{pmatrix} = \sum_{j=0}^{\infty} W_j(t) \cos\left(\frac{j\pi r}{r_n}\right) + \frac{r^2}{2r_n}\begin{pmatrix} 1 \\ 1 \end{pmatrix}, \tag{3.14}$$

where

$$W_0(t) = \begin{pmatrix} -\left[\frac{\beta_0}{6r_n(a+b)^2} + \frac{(a-b)r_n}{6(a+b)}\right] e^{-(a+b)t} + \frac{b\gamma_0 t}{6r_n(a+b)^2} + \frac{\beta_0}{6r_n(a+b)^2} - \frac{br_n}{3(a+b)} \\ \left[\frac{\beta_0}{6r_n(a+b)^2} + \frac{(a-b)r_n}{6(a+b)}\right] e^{-(a+b)t} + \frac{a\gamma_0 t}{6r_n(a+b)^2} - \frac{\beta_0}{6r_n(a+b)^2} - \frac{ar_n}{3(a+b)} \end{pmatrix},$$

with

$$\beta_0 = (b^2 - a^2)r_n^2 + 6a - 6ab, \quad \gamma_0 = 6(a+b)(1+\alpha),$$

and the higher Fourier coefficients $W_j(t)$ $(j > 0)$ are given in the Appendix.

It can checked that the series expansion (3.14) of $(D^{(0)}, V^{(0)})$ satisfies (3.7) for $g(t) = h(t) = 1$. Indeed, since

$$\int_0^{r_n} \cos\left(\frac{j\pi r}{r_n}\right) dr = 0, \quad j > 0,$$

we have

$$\begin{aligned} \int_0^{r_n} (D^{(0)} + V^{(0)}) dr &= \left[\frac{\gamma_0 t}{6r_n(a+b)} - \frac{r_n}{3}\right] \int_0^{r_n} dr + \int_0^{r_n} \frac{r^2}{r_n} dr, \\ &= \frac{\gamma_0 t}{6(a+b)}, \\ &= (1+\alpha)t. \end{aligned}$$

The extension to the more general case of time-dependent fluxes is stated next:

Corollary 1. *Let $g(t)$ and $h(t)$ be two smooth functions of t. Then a series solution of (3.10)–(3.13) can be written in the form*

$$\begin{pmatrix} D^{(0)}(r,t) \\ V^{(0)}(r,t) \end{pmatrix} = \sum_{j=0}^{\infty} W_j(t) \cos\left(\frac{j\pi r}{r_n}\right) + \frac{r^2}{2r_n}\begin{pmatrix} g(t) \\ h(t) \end{pmatrix},$$

where

$$W_j(t) = e^{tA_j} \int_0^t e^{-\tau A_j} Y_j(\tau) d\tau + e^{tA_j} W_j(0), \quad j \geq 0,$$

and the coefficients $W_j(0)$ and $Y_j(t)$ are given in the Appendix.

Proofs: The proofs of the theorem and corollary are lengthy and are therefore relegated to the Appendix.

4. **Numerical results for the full model.** In this section, we present numerical simulations of the full cellular model to investigate the kinetics of D_3 from the membrane to the nucleus, together with that of RANKL from the nucleus to the membrane. We also take this opportunity to test and validate the asymptotic solution, derived previously, against the numerical solution in the nucleus.

4.1. **Numerical methods.** The full cellular model (2.1)–(2.12) is solved numerically by a finite-difference method. Since it describes diffusion-dominated processes, we use a second-order implicit scheme of Crank–Nicolson type. Let

$$(u_a)_j^\delta = D_a(r_j, t_\delta), \quad (v_a)_j^\delta = V_a(r_j, t_\delta), \quad a = \{m, c, n\},$$

where $r_j = j\Delta r$ ($j = \{0, \ldots, J_a\}$) and $t_\delta = \delta\Delta t$ ($\delta = \{0, \ldots, I_a\}$).

In the membrane and cytoplasm ($a = \{m, c\}$), the discretized form of the bulk equation reads

$$\begin{aligned}\frac{(u_a)_j^{\delta+1} - (u_a)_j^\delta}{\Delta t} &= \kappa_a \left[\frac{(u_a)_{j+1}^{\delta+1} - 2(u_a)_j^{\delta+1} + (u_a)_{j-1}^{\delta+1}}{2(\Delta r)^2} \right. \\ &\quad \left. + \frac{(u_a)_{j+1}^{\delta} - 2(u_a)_j^{\delta} + (u_a)_{j-1}^{\delta}}{2(\Delta r)^2} \right].\end{aligned}$$

A similar discretized equation holds for v_a. In the nucleus ($a = n$), we have

$$\begin{aligned}\frac{(u_a)_j^{\delta+1} - (u_a)_j^\delta}{\Delta t} &= \kappa_a \left[\frac{(u_a)_{j+1}^{\delta+1} - 2(u_a)_j^{\delta+1} + (u_a)_{j-1}^{\delta+1}}{2(\Delta r)^2} \right. \\ &\quad \left. + \frac{(u_a)_{j+1}^{\delta} - 2(u_a)_j^{\delta} + (u_a)_{j-1}^{\delta}}{2(\Delta r)^2} \right] \\ &\quad - k_3 R_N (u_a)_j^{\delta+1} + k_4 (v_a)_j^{\delta+1} \\ &\quad + k_3 (u_a)_j^\delta (v_a)_j^\delta, \qquad (4.1) \\ \frac{(v_a)_j^{\delta+1} - (v_a)_j^\delta}{\Delta t} &= \kappa_{va} \left[\frac{(v_a)_{j+1}^{\delta+1} - 2(v_a)_j^{\delta+1} + (v_a)_{j-1}^{\delta+1}}{2(\Delta r)^2} \right. \\ &\quad \left. + \frac{(v_a)_{j+1}^{\delta} - 2(v_a)_j^{\delta} + (v_a)_{j-1}^{\delta}}{2(\Delta r)^2} \right] \\ &\quad + k_3 R_N (u_a)_j^{\delta+1} - k_4 (v_a)_j^{\delta+1} \\ &\quad - k_3 (u_a)_j^\delta (v_a)_j^\delta. \qquad (4.2)\end{aligned}$$

Note that the linear terms in (4.1)–(4.2) are treated implicitly while the nonlinear terms are treated explicitly. Otherwise, if all the terms were treated implicitly, we would need to solve a nonlinear system at each time step, which is a more demanding computational task. As mentioned in Section 3, we consider more particularly the regime of small concentrations in which the nonlinear contributions are weaker than the linear ones. Therefore, the explicit treatment of the nonlinear terms is not expected to significantly deteriorate the stability of the Crank–Nicolson scheme, provided the time step Δt is selected sufficiently small.

For the reflecting and transmission conditions, we use second-order backward and forward finite-difference formulas. For example, at the interface $r = r_m^i$ between

the cytoplasm and membrane (say at $j = j_1$), we have

$$\begin{aligned} & \kappa_m \frac{-(u_m)^\delta_{j_1+2} + 4(u_m)^\delta_{j_1+1} - 3(u_m)^\delta_{j_1}}{2\Delta r} \\ = \quad & \kappa_c \frac{3(u_c)^\delta_{j_1} - 4(u_c)^\delta_{j_1-1} + (u_c)^\delta_{j_1-2}}{2\Delta r}, \end{aligned}$$

and, at the interface $r = r_n$ between the nucleus and cytoplasm (say at $j = j_0$), we have

$$\begin{aligned} & \kappa_c \frac{-(u_c)^\delta_{j_0+2} + 4(u_c)^\delta_{j_0+1} - 3(u_c)^\delta_{j_0}}{2\Delta r} \\ = \quad & \kappa_n \frac{3(u_n)^\delta_{j_0} - 4(u_n)^\delta_{j_0-1} + (u_n)^\delta_{j_0-2}}{2\Delta r}. \end{aligned}$$

Similar formulas are used for v_a. In this way, the full numerical scheme is second order in both space and time.

Collecting all the discretized equations and expressing the resulting algebraic system in matrix form, we obtain

$$\mathbf{A}\mathbf{w}^{\delta+1} = \mathbf{B}\mathbf{w}^\delta + \mathbf{b}^\delta, \tag{4.3}$$

where

$$\mathbf{w}^\delta = (\mathbf{D_n}, \mathbf{D_c}, \mathbf{D_m}, \mathbf{V_n}, \mathbf{V_c}, \mathbf{V_m})^\top,$$

with

$$\begin{aligned} \mathbf{D_a} &= \left((u_a)^\delta_1, (u_a)^\delta_2, \ldots, (u_a)^\delta_{J_a}\right)^\top, \\ \mathbf{V_a} &= \left((v_a)^\delta_1, (v_a)^\delta_2, \ldots, (v_a)^\delta_{J_a}\right)^\top. \end{aligned}$$

The sparse vector $\mathbf{b}^\delta$ on the right-hand side of (4.3) contains contributions from the nonlinear terms in the nuclear model, and from the boundary condition (2.5)–(2.6) at the external surface of the membrane. The coefficient matrices $\mathbf{A}$ and $\mathbf{B}$ are sparse matrices resulting from the Crank–Nicolson discretization. Given the solution $\mathbf{w}^\delta$ at time t_δ, the solution $\mathbf{w}^{\delta+1}$ at the next time $t_{\delta+1}$ is found by solving the linear system (4.3) through direct Gaussian elimination.

4.2. **Discussion of numerical results.** Figure 4 shows snapshots of $D(r,t)$ and $V(r,t)$ over the entire cell, $0 < r < r^e_m$, at various times during the first two Ca^{2+} spikes (Figure 3). For graphical purposes, the relative sizes of the nucleus, cytoplasm and membrane are not imposed exactly. We particularly zoom in the nuclear region where the D-V interaction takes place. The variables are non-dimensionalized according to (3.4) with $\mathcal{D}_0 = 10^{-2}$, except that $\mathcal{R} = r^e_m$ so that $r \in [0,1]$ spans the entire cell. We choose $r_n = 0.4$ and $r^i_m = 0.8$. The computational domain is discretized into $J_a = 100$ grid points and the time step is set to be $\Delta t = 10^{-3}$.

We first observe that both curves are continuous across the whole domain at all times, which indicates that the transmission conditions at r_n (nucleus-cytoplasm interface) and r^i_m (cytoplasm-membrane interface) are well simulated by the numerical scheme. The difference in curve slope is representative of the different diffusivities specified in the three regions of the cell.

We clearly see that, as D diffuses in, it activates the production of V in the nucleus. During the increasing phase of the first Ca^{2+} spike ($t \lesssim 12$), the influx of D through the membrane is high and, accordingly, the ingoing diffusion is strong. Due to the reflecting boundary at $r = 0$, there is a gradual build-up of D in the nucleus, which persists even during the Ca^{2+} decreasing phase ($12 \lesssim t \lesssim 17$). On

the other hand, V steadily builds up in the nucleus during the whole Ca^{2+} spike, while diffusing out to the membrane. The successive increasing and decreasing phases of Ca^{2+} spiking are clearly indicated by the changes in D level at $r = r_m^e$. The zero Dirichlet boundary condition for V at $r = r_m^e$, corresponding to instant diffusion out of the cell, is also well reproduced numerically.

During the second Ca^{2+} spike ($17 \lesssim t \lesssim 29$), this reaction-diffusion process repeats itself. The new influx further raises the D concentration in the nucleus before it has a chance to diffuse all out. As a result, more V is created there. This suggests that tying the boundary conditions to the calcium spikes may not be correct and that a more complicated mechanical procedure is necessary to monitor the intake of D_3, such as receptor-mediated endocis or perhaps through the closing and snipping of caveolae suggested earlier. These models will be investigated in a future work. Note the resemblance of concentration profiles for D between $t = 20$ and $t = 30$ which correspond to a periodic Ca^{2+} cycle (Figure 3). In contrast, the V concentration in the nucleus continually increases during those two Ca^{2+} spikes. It remains five orders of magnitude lower than the D concentration up to $t = 30$. According to our non-dimensionalization (3.4), the typical diffusion time through the cell is $O(1)$. Therefore, the simulation time up to $t = 30$ is sufficiently long to illustrate the reaction-diffusion process between D and V through the entire cell during at least two Ca^{2+} spikes.

Furthermore, a version of the numerical scheme described in the previous section, was implemented to solve the nuclear model (3.5)–(3.6) with $g(t) = h(t) = 1$, in view of testing the asymptotic solution $(D^{(0)}, V^{(0)})$ of Theorem 3.2. Figure 5 shows the comparison between the asymptotic and numerical solutions (for both D and V) at various times. Here we choose $\mathcal{R} = r_n$ so that $r \in [0, 1]$ only spans the nucleus. Again $J_a = 100$ and $\Delta t = 10^{-3}$. A number of 10 terms is used in the Fourier series (3.14) of $(D^{(0)}, V^{(0)})$. Overall, an excellent agreement is found. After $t = 1$, the asymptotic and numerical curves are indistinguishable at the graphical scale of Figure 5. This result not only verifies the derivation of our asymptotic solution, but also validates *a posteriori* the choice of ϵ as the perturbation parameter in our asymptotic calculations, and hence it validates the choice of the scaling regime defined by (3.4).

We also note from Figure 5 that the amplitude of both D and V keeps increasing with time, which is consistent with the fact that the first Fourier coefficient W_0 in the asymptotic solution tends to grow linearly with t as $t \to +\infty$ (see Theorem 3.2). In contrast, the higher Fourier coefficients W_j ($j > 0$) decay exponentially in time because the corresponding eigenvalues $\lambda_j^{\pm}$ are all negative (see Eq. (6.10) in the Appendix). The characteristic parabolic curve for both D and V is reminiscent of the term $r^2/(2r_n)$ in the asymptotic solution, which accommodates the Neumann boundary conditions (3.13) at $r = 0$ and $r = r_n$.

The growth of D and V in the nucleus is further revealed in Figure 6 which shows numerical values of $E(t)$ as a function of time. The trapezoidal rule was used to evaluate the integral in r. According to Theorem 3.1, $E(t)$ grows linearly with t at rate $1 + \alpha$ for $g(t) = h(t) = 1$. This behavior is well reproduced by the numerical solution, as indicated by the excellent agreement observed in Figure 6.

Finally, the convergence of the Fourier series (3.14) in $(D^{(0)}, V^{(0)})$ is examined in Figure 7 which plots the relative L_2 error between the asymptotic and numerical solutions in the nucleus at $t = 0.01$ and $t = 10$, as a function of the number of terms in the series. Overall, the errors for D and V are both found to be very

small. At $t = 0.01$ (early time), they rapidly decrease as the number of terms in the series increases, to plateau around 10^{-2}. At $t = 10$ (later time), these errors remain pretty much constant around 10^{-4}. This result is not surprising since, as mentioned above, the first term W_0 tends to prevail as t increases. The higher terms ($j > 0$) decay exponentially with t and thus, very quickly, do not contribute further to the convergence of the Fourier series.

5. **Conclusions.** In this paper, we have provided a simplified mathematical model of the pre-osteoblastic cell. We have indicated where this model deviates from the biological system. To our knowledge, this is the first time the entire process of entry of D_3 through the membrane and across the cytoplasm into the nucleus, and the transcription of the gene encoding receptor activator of RANKL, has been mathematically modeled. The graphs indicate the arrival times of D_3 and the exit times of RANKL through the membrane. Arrival time in the nucleus is usually too quick compared with the only known experimental data presented in [3]. This can be fixed using an idea discussed in [18] where an effective diffusivity is introduced. This uses the method of homogenization with which we are well aware of ([6, 7] and the references therein). Another important finding in [19] was the approximate formula for the effective diffusion coefficient

$$D^H = D_0 \left(1 - \frac{\phi}{\phi_c}\right)^{\alpha\phi_c}, \tag{5.1}$$

where D_0 is the diffusion coefficient of the solvent, ϕ is the volume fraction of obstacles, ϕ_c is the critical volume fraction that is the minimal volume fraction of obstacles at which a tracer particle is trapped, and α is the empirical constant. This is one possible way in which to correct the arrival time. Another is to distribute the transport from a purely diffusional process to one in which D_3 diffuses until meeting a microtubule and then is transported to the nuclear pore. This would require a more complicated geometry than used here. Numerical experiments conducted in [19] show that, for all relevant volume fractions, (5.1) agrees very well with the effective diffusion obtained by the classical homogenization procedure (see e.g. [8]). Our tying of the boundary conditions for D_3 at the membrane surface to the production of calcium waves was rather simplistic. We could rather choose to have the entry of a calcium spike instigating a probabilistic procedure for the passing of a quantity of D_3 across the membrane. This is envisioned for future work.

Acknowledgments. This work was funded in part by the National Science Foundation through Mathematical Biology grant No. DMS-0920850 and by a grant from the Simons Foundation (No. 246170 to P. Guyenne). P. Guyenne would also like to thank the Institute for Advanced Study (Princeton, NJ) for its hospitality during the academic year 2011–2012.

6. **Appendix.**

6.1. **Proof of Theorem 3.2.** In this section, we give details on the proof of Theorem 3.2.

We examine the problem (3.10)–(3.13) with $g(t) = h(t) = 1$. The non-homogeneous boundary conditions (3.13) suggest the change of variables

$$D^{(0)}(r,t) = u(r,t) + \frac{r^2}{2r_n},$$
$$V^{(0)}(r,t) = v(r,t) + \frac{r^2}{2r_n},$$

so Eqs. (3.10)–(3.13) become

$$\frac{\partial u}{\partial t} = \frac{\partial^2 u}{\partial r^2} - au + bv - (a-b)\frac{r^2}{2r_n} + \frac{1}{r_n}, \tag{6.1}$$
$$\frac{\partial v}{\partial t} = \alpha\frac{\partial^2 v}{\partial r^2} + au - bv + (a-b)\frac{r^2}{2r_n} + \frac{\alpha}{r_n}, \tag{6.2}$$

with initial conditions

$$u(r,0) = v(r,0) = -\frac{r^2}{2r_n}, \tag{6.3}$$

and homogeneous boundary conditions

$$\frac{\partial u}{\partial r}(0,t) = \frac{\partial v}{\partial r}(0,t) = 0, \quad \frac{\partial u}{\partial r}(r_n,t) = \frac{\partial v}{\partial r}(r_n,t) = 0. \tag{6.4}$$

By the superposition principle and separation of variables, we look for a solution of (6.1)–(6.4) in terms of Fourier cosine series

$$u(r,t) = \sum_{j=0}^{\infty} u_j(t)\cos\left(\frac{j\pi r}{r_n}\right),$$
$$v(r,t) = \sum_{j=0}^{\infty} v_j(t)\cos\left(\frac{j\pi r}{r_n}\right),$$

which satisfy (6.4). Plugging these expressions in (6.1)–(6.2), we obtain

$$u_0' = -au_0 + bv_0 + \frac{1}{r_n} - (a-b)\frac{r_n}{6}, \tag{6.5}$$
$$v_0' = au_0 - bv_0 + \frac{\alpha}{r_n} + (a-b)\frac{r_n}{6}, \tag{6.6}$$

for $j = 0$, and

$$u_j' = -\left(a + \frac{j^2\pi^2}{r_n^2}\right)u_j + bv_j - \frac{2(-1)^j(a-b)r_n}{j^2\pi^2}, \tag{6.7}$$
$$v_j' = au_j - \left(b + \alpha\frac{j^2\pi^2}{r_n^2}\right)v_j + \frac{2(-1)^j(a-b)r_n}{j^2\pi^2}, \tag{6.8}$$

for $j \geq 1$, where we have used

$$\frac{r^2}{2r_n} = \frac{r_n}{6} + \sum_{j=1}^{\infty}\frac{2(-1)^j r_n}{j^2\pi^2}\cos\left(\frac{j\pi r}{r_n}\right), \tag{6.9}$$

and the primes stand for differentiation. Let

$$W_j(t) = \begin{pmatrix} u_j(t) \\ v_j(t) \end{pmatrix}, \quad A_j = \begin{pmatrix} -a-\sigma_j & b \\ a & -b-\alpha\sigma_j \end{pmatrix}, \quad \sigma_j = \frac{j^2\pi^2}{r_n^2},$$

for $j \geq 0$, and

$$B_0 = \begin{pmatrix} \frac{1}{r_n} - \frac{(a-b)r_n}{6} \\ \frac{\alpha}{r_n} + \frac{(a-b)r_n}{6} \end{pmatrix}, \quad B_j = \frac{2(-1)^j(a-b)r_n}{j^2\pi^2} \begin{pmatrix} -1 \\ 1 \end{pmatrix},$$

for $j \geq 1$. The eigenvalues of A_j are

$$\lambda_j^{\pm} = \frac{1}{2}\left(-p_j \pm \sqrt{p_j^2 - 4q_j}\right),$$

with

$$p_j = (1+\alpha)\sigma_j + a + b, \quad q_j = (\alpha\sigma_j + b + \alpha a)\sigma_j,$$

and, in particular, they reduce to $\lambda_0^+ = 0$ and $\lambda_0^- = -(a+b)$ for $j = 0$. For $j > 0$, both $\lambda_j^{\pm} < 0$ because the parameters a, b, α and σ_j are all positive. These evanescent modes are representative of the underlying diffusion process.

Equations (6.5)–(6.6) can be rewritten as

$$W_0' = A_0 W_0 + B_0,$$

whose solution is given by

$$W_0(t) = e^{tA_0}\left(\int_0^t e^{-\tau A_0} B_0 d\tau + C_0\right),$$

using the integrating factor technique. By diagonalization,

$$e^{\pm tA_0} = \frac{1}{a+b}\begin{pmatrix} b + a\,e^{\mp(a+b)t} & b - b\,e^{\mp(a+b)t} \\ a - a\,e^{\mp(a+b)t} & a + b\,e^{\mp(a+b)t} \end{pmatrix},$$

and thus

$$W_0(t) = \frac{1}{6r_n(a+b)^2}\begin{pmatrix} -\beta_0 e^{-(a+b)t} + b\gamma_0 t + \beta_0 \\ \beta_0 e^{-(a+b)t} + a\gamma_0 t - \beta_0 \end{pmatrix} + e^{tA_0} C_0,$$

where

$$\beta_0 = (b^2 - a^2)r_n^2 + 6a - 6ab, \quad \gamma_0 = 6(a+b)(1+\alpha).$$

The constant of integration

$$C_0 = W_0(0) = -\frac{r_n}{6}\begin{pmatrix} 1 \\ 1 \end{pmatrix},$$

is determined from the initial condition (6.3) together with the first term of the Fourier series (6.9). Collecting all the contributions, we find

$$W_0(t) = \begin{pmatrix} -\left[\frac{\beta_0}{6r_n(a+b)^2} + \frac{(a-b)r_n}{6(a+b)}\right] e^{-(a+b)t} + \frac{b\gamma_0 t}{6r_n(a+b)^2} + \frac{\beta_0}{6r_n(a+b)^2} - \frac{br_n}{3(a+b)} \\ \left[\frac{\beta_0}{6r_n(a+b)^2} + \frac{(a-b)r_n}{6(a+b)}\right] e^{-(a+b)t} + \frac{a\gamma_0 t}{6r_n(a+b)^2} - \frac{\beta_0}{6r_n(a+b)^2} - \frac{ar_n}{3(a+b)} \end{pmatrix}.$$

Similarly, Eqs. (6.7)–(6.8) for $j \geq 1$ can be expressed as

$$W_j' = A_j W_j + B_j,$$

whose solution is given by

$$W_j(t) = e^{tA_j}\left(\int_0^t e^{-\tau A_j} B_j d\tau + C_j\right),$$

where

$$C_j = W_j(0) = \frac{2(-1)^{j+1} r_n}{j^2\pi^2}\begin{pmatrix} 1 \\ 1 \end{pmatrix},$$

as derived from the Fourier coefficients of (6.9), and

$$e^{\pm tA_j} = \frac{1}{\lambda_j^+ - \lambda_j^-} \begin{pmatrix} -m_j^- e^{\pm\lambda_j^+ t} + m_j^+ e^{\pm\lambda_j^- t} & b(e^{\pm\lambda_j^+ t} - e^{\pm\lambda_j^- t}) \\ -\frac{m_j^+ m_j^-}{b}(e^{\pm\lambda_j^+ t} - e^{\pm\lambda_j^- t}) & m_j^+ e^{\pm\lambda_j^+ t} - m_j^- e^{\pm\lambda_j^- t} \end{pmatrix}, \quad (6.10)$$

with

$$m_j^\pm = \lambda_j^\pm + \sigma_j + a.$$

This leads to

$$\begin{aligned} I_j &= \int_0^t e^{-\tau A_j} B_j d\tau, \\ &= \frac{2(-1)^j (a-b) r_n}{(\lambda_j^+ - \lambda_j^-) j^2 \pi^2} \\ &\times \begin{pmatrix} -\frac{m_j^- + b}{\lambda_j^+} e^{-\lambda_j^+ t} + \frac{m_j^+ + b}{\lambda_j^-} e^{-\lambda_j^- t} + \frac{m_j^- + b}{\lambda_j^+} - \frac{m_j^+ + b}{\lambda_j^-} \\ -\frac{m_j^+ m_j^- + b m_j^+}{b\lambda_j^+} e^{-\lambda_j^+ t} + \frac{m_j^+ m_j^- + b m_j^-}{b\lambda_j^-} e^{-\lambda_j^- t} + \frac{m_j^+ m_j^- + b m_j^+}{b\lambda_j^+} - \frac{m_j^+ m_j^- + b m_j^-}{b\lambda_j^-} \end{pmatrix}, \end{aligned}$$

so that

$$W_j(t) = e^{tA_j} I_j + e^{tA_j} W_j(0).$$

Therefore

$$\begin{pmatrix} D^{(0)}(r,t) \\ V^{(0)}(r,t) \end{pmatrix} = \sum_{j=0}^{\infty} W_j(t) \cos\left(\frac{j\pi r}{r_n}\right) + \frac{r^2}{2r_n} \begin{pmatrix} 1 \\ 1 \end{pmatrix},$$

which completes the proof of the theorem. □

We remark that the next-order terms in the power-series solution (3.8)–(3.9) can be determined in a similar way, however this procedure becomes increasingly more tedious.

6.2. **Proof of Corollary 1.** Here we present the proof of Corollary 1 which deals with the more general case of time-dependent fluxes through the surface of the nucleus.

The main steps are similar to those for the proof of Theorem 3.2. The non-homogeneity of (3.13) is taken care of by decomposing

$$\begin{aligned} D^{(0)}(r,t) &= u(r,t) + \frac{r^2}{2r_n} g(t), \\ V^{(0)}(r,t) &= v(r,t) + \frac{r^2}{2r_n} h(t). \end{aligned}$$

The auxiliary functions u and v satisfy

$$\begin{aligned} \frac{\partial u}{\partial t} &= \frac{\partial^2 u}{\partial r^2} - au + bv + s(r,t), \\ \frac{\partial v}{\partial t} &= \alpha \frac{\partial^2 v}{\partial r^2} + au - bv + z(r,t), \end{aligned}$$

$$u(r,0) = -\frac{r^2}{2r_n} g(0), \quad v(r,0) = -\frac{r^2}{2r_n} h(0),$$

$$\frac{\partial u}{\partial r}(0,t) = \frac{\partial v}{\partial r}(0,t) = 0, \quad \frac{\partial u}{\partial r}(r_n,t) = \frac{\partial v}{\partial r}(r_n,t) = 0, \quad (6.11)$$

where

$$\begin{aligned} s(r,t) &= \left(\frac{1}{r_n} - \frac{ar^2}{2r_n}\right) g(t) - \frac{r^2}{2r_n} g'(t) + \frac{br^2}{2r_n} h(t), \\ z(r,t) &= \left(\frac{\alpha}{r_n} - \frac{br^2}{2r_n}\right) h(t) - \frac{r^2}{2r_n} h'(t) + \frac{ar^2}{2r_n} g(t). \end{aligned}$$

Given the homogeneous boundary conditions (6.11), we assume the possibility of writing u and v as Fourier cosine series

$$\begin{aligned} u(r,t) &= \sum_{j=0}^{\infty} u_j(t) \cos\left(\frac{j\pi r}{r_n}\right), \\ v(r,t) &= \sum_{j=0}^{\infty} v_j(t) \cos\left(\frac{j\pi r}{r_n}\right), \end{aligned}$$

and, similarly,

$$\begin{aligned} s(r,t) &= \sum_{j=0}^{\infty} s_j(t) \cos\left(\frac{j\pi r}{r_n}\right), \\ z(r,t) &= \sum_{j=0}^{\infty} z_j(t) \cos\left(\frac{j\pi r}{r_n}\right), \end{aligned}$$

where

$$\begin{aligned} s_j(t) &= \frac{2}{r_n} \int_0^{r_n} s(r,t) \cos\left(\frac{j\pi r}{r_n}\right) dr, \\ z_j(t) &= \frac{2}{r_n} \int_0^{r_n} z(r,t) \cos\left(\frac{j\pi r}{r_n}\right) dr, \quad j \geq 0, \end{aligned}$$

while the u_j and v_j's obey

$$u_j' = -(a+\sigma_j)u_j + bv_j + s_j, \tag{6.12}$$

$$v_j' = au_j - (b+\alpha\sigma_j)v_j + z_j, \tag{6.13}$$

given

$$\sigma_j = \frac{j^2\pi^2}{r_n^2}.$$

Let

$$W_j(t) = \begin{pmatrix} u_j(t) \\ v_j(t) \end{pmatrix}, \quad A_j = \begin{pmatrix} -a-\sigma_j & b \\ a & -b-\alpha\sigma_j \end{pmatrix}, \quad Y_j(t) = \begin{pmatrix} s_j(t) \\ z_j(t) \end{pmatrix},$$

for $j \geq 0$. Equations (6.12)–(6.13) then read

$$W_j' = A_j W_j + Y_j,$$

which can be solved by the integrating factor technique, yielding

$$W_j(t) = e^{tA_j} \int_0^t e^{-\tau A_j} Y_j(\tau) d\tau + e^{tA_j} W_j(0),$$

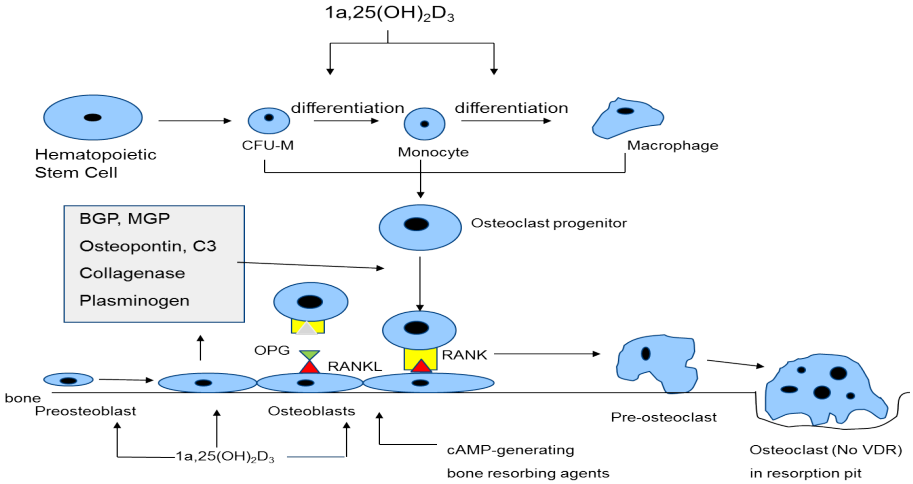

FIGURE 1. Dynamics of vitamin D_3 on a preosteoblast (courtesy of Dr. Anja Nohe).

where the exponentials $e^{\pm tA_j}$ are defined by (6.10) and $W_j(0) = (u_j(0), v_j(0))^\top$ is determined from the initial conditions

$$\begin{aligned} u(r,0) &= -\frac{r^2}{2r_n} g(0) = \sum_{j=0}^{\infty} u_j(0) \cos\left(\frac{j\pi r}{r_n}\right), \\ v(r,0) &= -\frac{r^2}{2r_n} h(0) = \sum_{j=0}^{\infty} v_j(0) \cos\left(\frac{j\pi r}{r_n}\right). \end{aligned}$$

Hence

$$\begin{aligned} u_j(0) &= \frac{2}{r_n} \int_0^{r_n} \left(-\frac{r^2}{2r_n} g(0)\right) \cos\left(\frac{j\pi r}{r_n}\right) dr, \\ v_j(0) &= \frac{2}{r_n} \int_0^{r_n} \left(-\frac{r^2}{2r_n} h(0)\right) \cos\left(\frac{j\pi r}{r_n}\right) dr. \end{aligned}$$

This concludes the proof of the corollary. □

REFERENCES

[1] A. Atri, J. Amundson, D. Clapham and J. Sneyd, *A single-pool model for intracellular calcium oscillations and waves in the Xenopus laevis Oocyte*, Biophys. J., **65** (1993), 1727–1739.

[2] F. Bronner, *Cytoplasmic transport of calcium and other inorganic ions*, Comp. Biochem. Physiol., **115B** (1996), 313–317.

[3] J. Buchanan, R. P. Gilbert and M. J. Ou, *The kinetics of vitamin D_3 in the osteoblastic cell*, Submitted to J. Theor. Biol., (2012).

[4] E. M. Costa and D. Feldman, *Measurement of 1,25-Dihydroxyvitamin D3 receptor turnover by dense amino acid labeling: Changes during receptor up-regulation by vitamin D metabolites*, Endocrinology, **120** (1987), 1173–1178.

[5] M. C. Farach-Carson and P. J. Davis, *Steroid hormone interactions with target cells: Cross talk between membrane and nuclear pathways*, J. Pharm. Exp. Therap., **307** (2003), 839–845.

[6] R. Gilbert, A. Panasenko and A. Vasilic, *Acoustic Propagation in a Random Saturated Medium: The Monophasic Case*, Math. Mehods Appl. Sciences, **33** (2010), 2206–2214.

[7] K. Hackl and S. Ilic, *Application of the multiscale FEM to the modeling of cancellous bone*, Biomechan. Model. Mechanobiol., **9** (2010), 87–102.

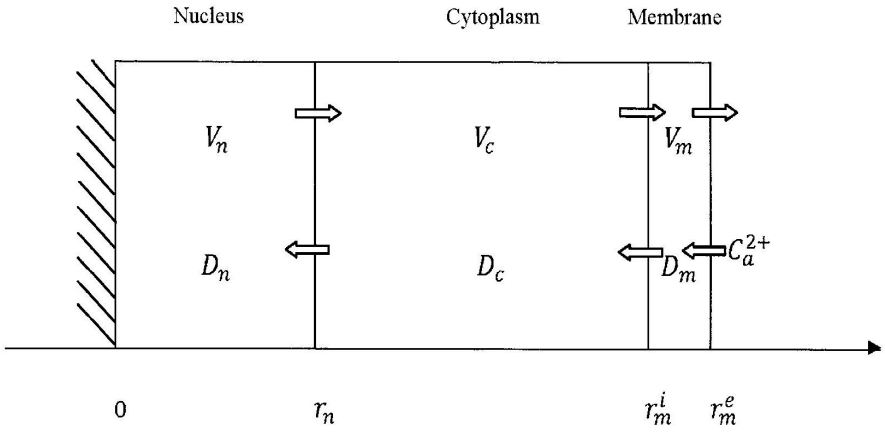

FIGURE 2. Sketch of the cellular model with all the components involved.

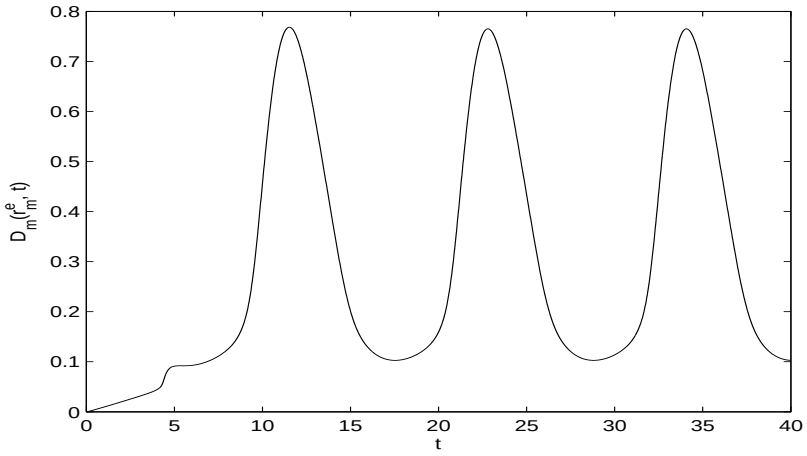

FIGURE 3. Effective D_3 concentration at the external membrane surface $r = r_m^e$ as given by the boundary conditions (2.5)–(2.7).

[8] V. V. Jikov, S. M. Kozlov and O.A. Oleinik, "Homogenization of Differential Operators and Integral Functionals," Springer, Berlin 1994.
[9] J. Keener and J. Sneyd, "Mathematical Physiology," Springer, Berlin, 1998.
[10] S. V. Komarova, R. J. Smith, S. J. Dixon, S. M. Sims and L. M. Wahl, *Mathematical model predicts a critical role for osteoclast autocrine regulation in the control of bone remodeling*, Bone, **33** (2003), 206–215.
[11] D. L. Lacey, E. Timms, h.-L. Tan, M. J. Kelley, C. R. Dunstan, T. Burgess, R. Elliott, A. Columbero, G. Elliott, S. Scully, H. Hsu, J. Sullivan, N. Hawkins, E. Davy, C. Capparelli, A. Eli, Y. X. Qian, S. Kaufman, I. Sarosi, V. Shalhoub, G. Senaldi, J. Guo, J. Delaney and W. J. Boyle, *Osteoprotegerin ligand is a cytokine that regulates osteoclast differentiation and activation*, Cell, **93** (1998), 165–176.
[12] D. A. Lauffenburger and J. Linderman, "Receptors: Models for Binding, Trafficking and Signaling," Oxford University Press, New York, 1996.

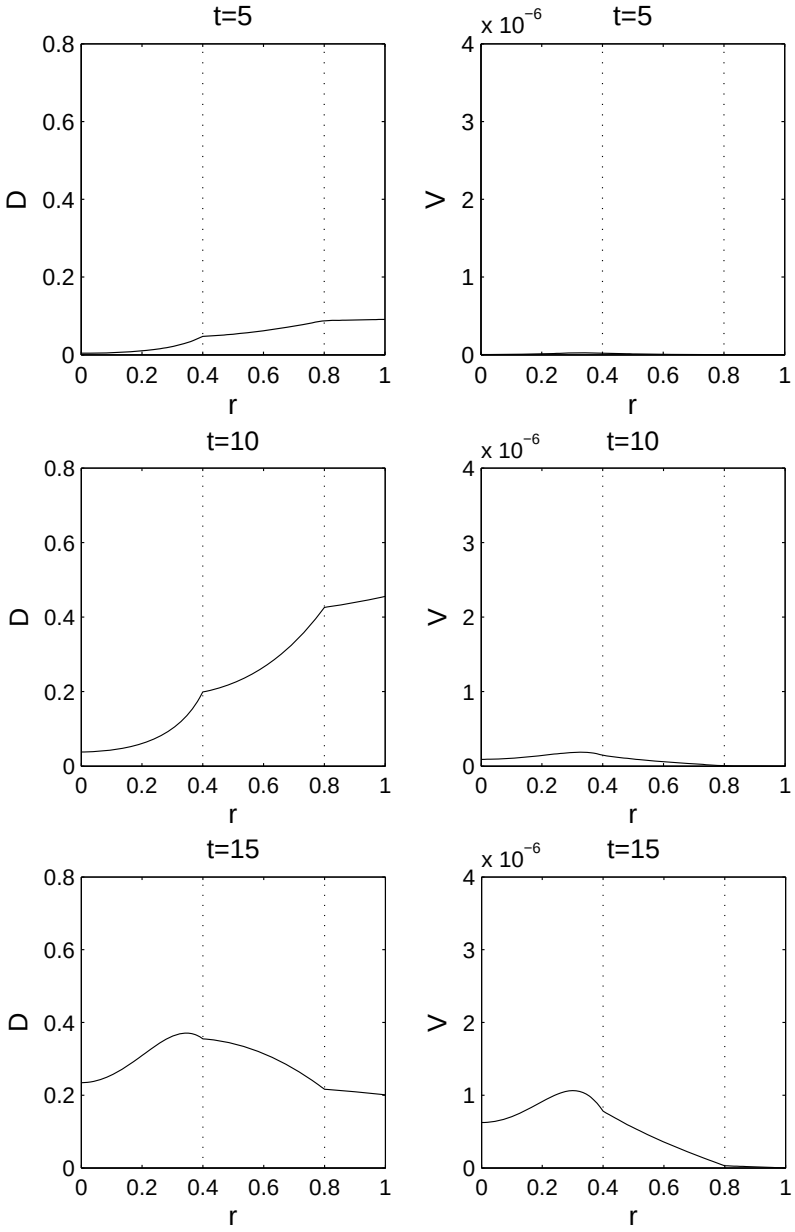

See next page for caption.

[13] V. Lemaire, F. L. Tobin, L. D. Greller, C. R. Cho and L. J. and Suva, *Modeling the interactions between osteoblast and osteoclast activities in bone remodeling*, J. Theor. Biol., **229** (2004), 293–309.

[14] I. Nemere, *24,25-Dihydroxyvitamin D3 suppresses the rapid actions of 1,25 Dihydroxyvitamin D3 and parathyroid hormone on calcium transport in chick intestine*, Bone Miner. Res., **14** (1999), 1543–1549.

[15] I. Nemere, N. Garbi, G. J. Hammerling and R. C. Khanal, *Intestinal cell calcium uptake and the targeted knockout of the 1,25D3-MARRS (Membrane-associated, rapid response steroid-binding) receptor/PDIA3/Erp57*, J. Biol. Chem., **285** (2010), 31859–31866.

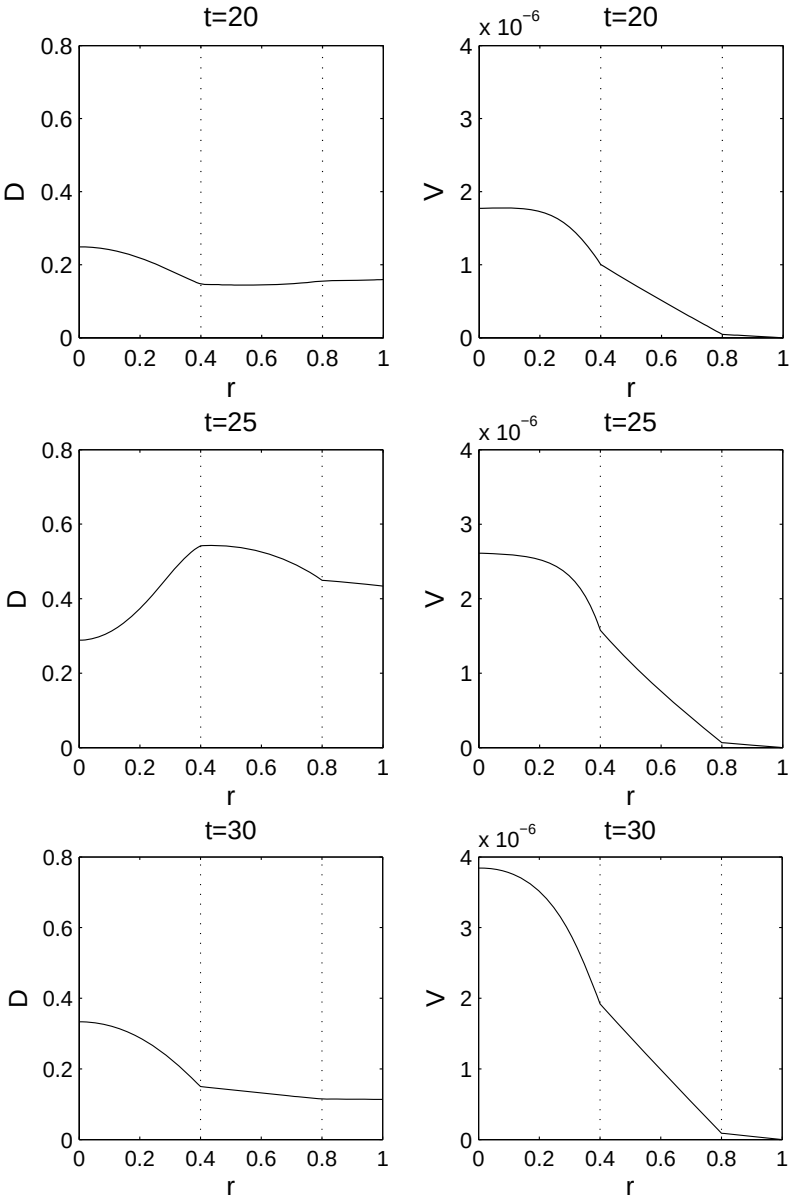

FIGURE 4. Snapshots of D (left) and V (right) over the entire cell ($0 \le r \le r_m^e = 1$) at $t = 5$, 10, 15, 20, 25 and 30. The vertical dotted lines at $r = r_n = 0.4$ and $r = r_m^i = 0.8$ separate the three regions of the cell (nucleus, cytoplasm and membrane).

[16] I. Nemere, R. J. Pietras and P. F. Blackmore, *Membrane receptors for membrane hormones: Signal transduction and physiological significance*, J. Cell Biochem., **88** (2003), 438–445.

[17] A. W. Norman, "Rapid Biological Responses Mediated by $1\alpha, 25$-Dihydroxyvitamin D_3," In Vitamin D (D. Feldman and F. H. Glorieux and J. W. Pike), Academic Press, New York, 1997.

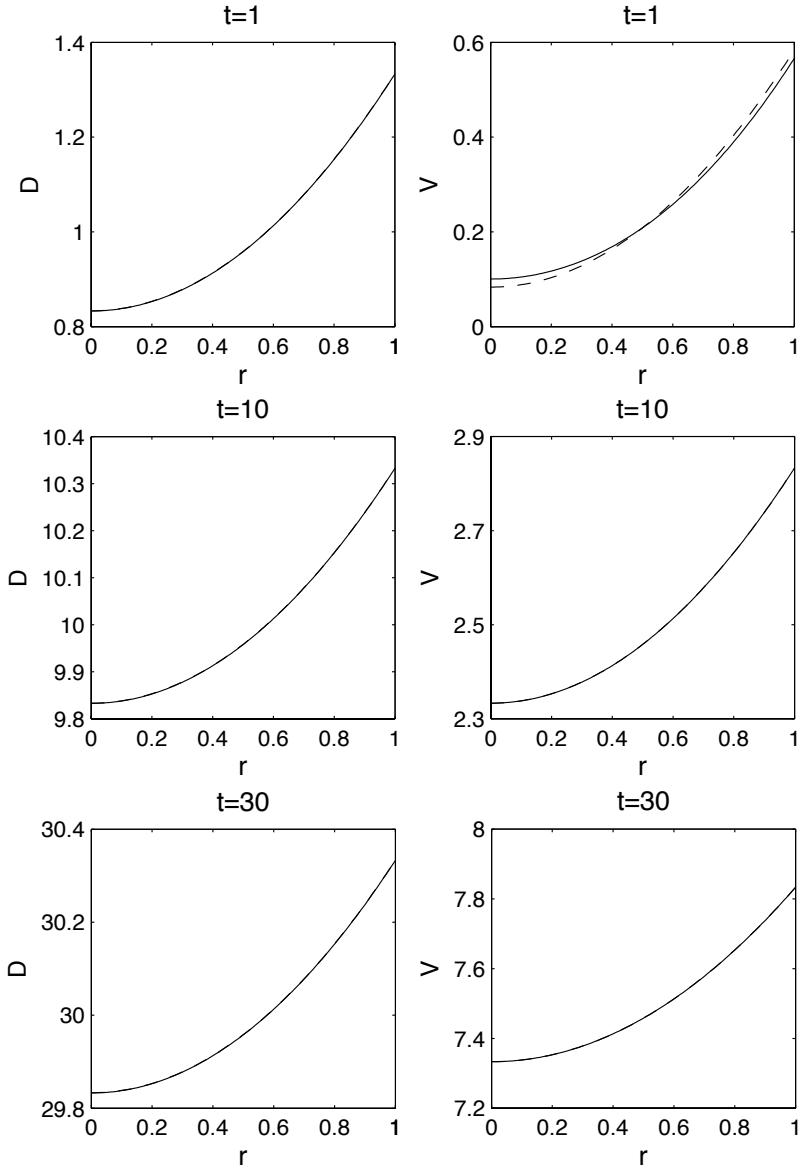

FIGURE 5. Comparison between the numerical (solid line) and asymptotic (dashed line) solutions for D (left) and V (right) in the nucleus ($0 \leq r \leq r_n = 1$) at $t = 1$, 10 and 30.

[18] I. Novak, P. Kraikivski and B. Slepchenko, *Diffusion in cytoplasm: Effects of excluded volume due to internal membranes and cytoskeletal structures*, Biophys. J., **97** (2009), 758–767.

[19] I. L. Novak, F. Gao, P. Kraikivski and B. Slepchenko, *B. M. Diffusion amid random overlapping obstacles: Similarities, invariants, aproximations*, J. Chem. Phys., **134** (2011), 154104.

[20] J. W. Pike, "The Vitamin D Receptor and Its Gene," In Vitamin D (D. Feldman, F. H. Glorieux and J. W. Pike), Academic Press, New York, 1997, 105–125.

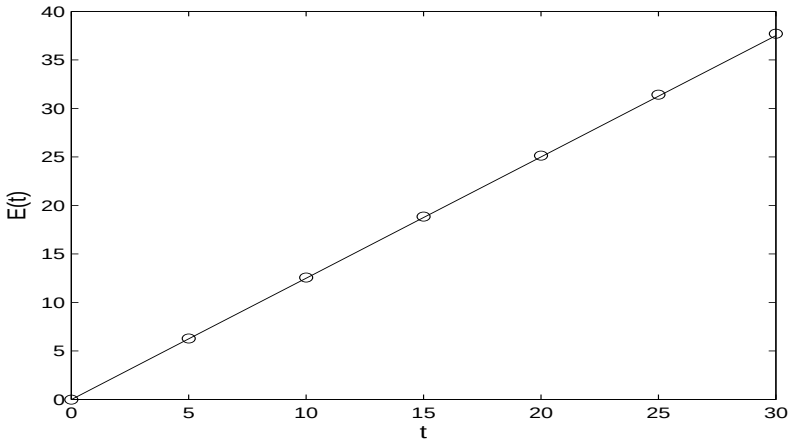

FIGURE 6. Numerical values of $E(t)$ as a function of time (circles). For comparison, the theoretical curve $(1+\alpha)t$, with $\alpha = 0.25$, is also plotted in solid line.

[21] W. S. Simonet, D. L. Lacey, C. R. Dunstan, M. Kelley, M.-S. Chang, R. Lothy, H. Q. Nguyen, S. Wooden, L. Bennett, T. Boone, G. Shimamoto, M. DeRose, R. Elliott, A. Columbero, H.-L. Tan, G. Trail, J. Sullivan, E. Davy, N. Bucay, L. Renshaw-Gregg, T. M. Hughes, D. Hill, W. Pattison, P. Campbell, S. Sander, G. Van, J. Tarpley, P. Derby, R. Lee and W. J. Boyle, *Osteoprotegerin: A novel secreted protein involved in the regulation of bone density*, Cell, **89** (1997), 309–319.

[22] P. Slepchenko, I. Semenova, I. Zaliopin. and V. Rodianaov, *Switching of membrane organelles between cytoskeletal transport systems is determined by regulation of the microtubule-based transport*, J. Cell Biol., **179** (2007), 635–641.

[23] G. K. Witfield, P. W. Jurutka, C. A. Hausler, J.-C. Hsieh, T. K. Barthel, E. T. Jacobs, C. E. Dominguez, M. L. Thatcher and M. R. Hausler, "Nuclear Vitamin D Receptor: Control of Gene Transcription, and Novel Bioactions," In Vitamin D (D. Feldman, F. H. Glorieux and J. W. Pike), Academic Press, New York, 1997, 219–261.

Received May 06, 2012; Accepted November 16, 2012.

E-mail address: gilbert@math.udel.edu
E-mail address: guyenne@math.udel.edu
E-mail address: liuy@math.udel.edu

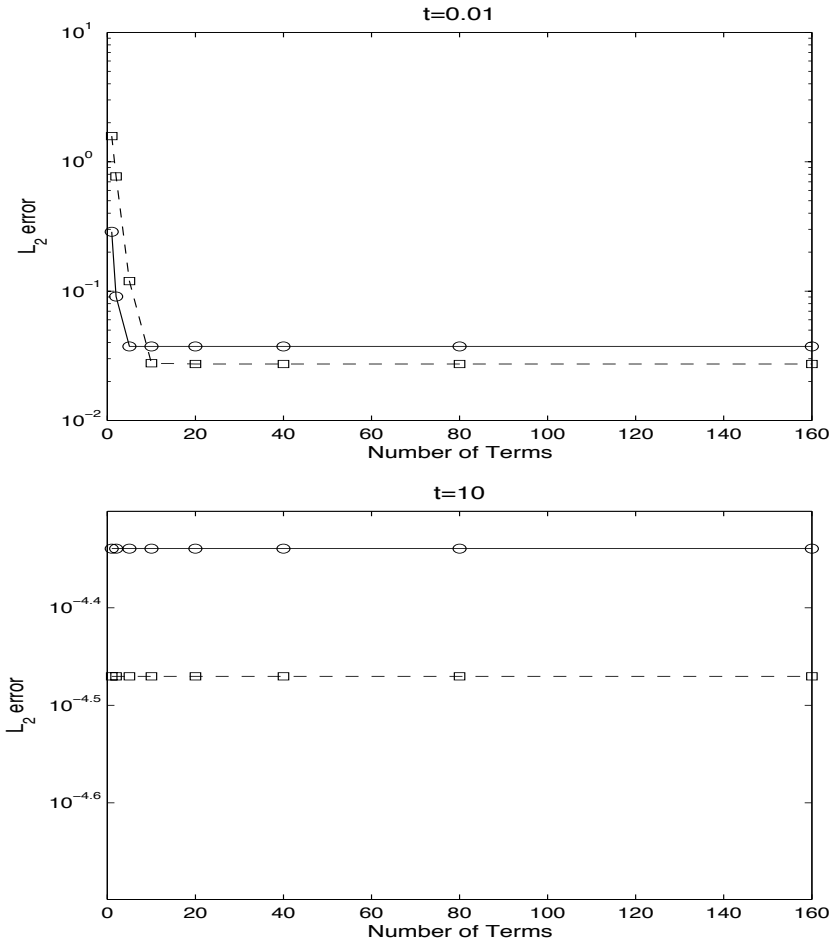

FIGURE 7. Relative L_2 error between the asymptotic and numerical solutions in the nucleus at $t = 0.01$ (top) and $t = 10$ (bottom), as a function of the number of terms in the Fourier series. The solid line (resp. dashed line) corresponds to D (resp. V). Values for 1 up to 160 terms are plotted.